# Bundled Assembly of Helical Nanostructures in Polymeric Micelles Loaded with Platinum Drugs Enhancing Therapeutic Efficiency against Pancreatic Tumor

**Yuki Mochida,[†] Horacio Cabral,[†] Yutaka Miura,[‡] Francesco Albertini,[§] Shigeto Fukushima,[⊥] Kensuke Osada,[†,∥] Nobuhiro Nishiyama,[#,*] and Kazunori Kataoka[†,‡,⊥,*]**

[†]Department of Bioengineering, Graduate School of Engineering, The University of Tokyo, 7-3-1 Hongo, Bunkyo-ku, Tokyo 113-8656, Japan, [‡]Division of Clinical Biotechnology, Center for Disease Biology and Integrative Medicine, Graduate School of Medicine, The University of Tokyo, 7-3-1 Hongo, Bunkyo-ku, Tokyo 113-0033, Japan, [§]Department of Materials, Swiss Federal Institute of Technology Zürich, Wolfgang-Pauli-Strasse 10, CH-8093 Zürich, Switzerland, [⊥]Department of Materials Engineering, Graduate School of Engineering, The University of Tokyo, 7-3-1 Hongo, Bunkyo-ku, Tokyo 113-8656, Japan, [∥]Japan Science and Technology Agency, PRESTO, 4-1-8 Honcho, Kawaguchi, Saitama 332-0012, Japan, and [#]Polymer Chemistry Division, Chemical Resources Laboratory, Tokyo Institute of Technology, R1-11, 4259 Nagatsuta, Midori-ku, Yokohama 226-8503, Japan

**ABSTRACT** Supramolecular assemblies of amphiphilic block copolymers having polypeptide segments offer significant advantages for tailoring spatial arrangement based on secondary structures in their optically active backbones. Here, we demonstrated the critical effect of α-helix bundles in cisplatin-conjugated poly(L- (or D-)glutamate) [P(L(or D)Glu)-CDDP] segment on the packaging of poly(ethylene glycol) (PEG)-P(L(or D)Glu)-CDDP block copolymers in the core of polymeric micelles (CDDP/m) and enhanced micelle tolerability to harsh *in vivo* conditions for accomplishing appreciable antitumor efficacy against intractable pancreatic tumor by systemic injection. CDDP/m prepared from optically inactive PEG-poly(D,L-glutamate) (P(D,LGlu)), gradually disintegrated in the bloodstream, resulting in increased accumulation in liver and spleen and reduced antitumor efficacy. Alternatively, CDDP/m from optically active PEG-P(L(or D)Glu) maintained micelle structure during circulation, and eventually attained selective tumor accumulation while reducing nonspecific distribution to liver and spleen. Circular dichroism and small-angle X-ray scattering measurements indicated regular bundled assembly of α-helices in the core of CDDP/m from PEG-P(L(or D)Glu), which is suggested to stabilize the micelle structure against dilution in physiological condition. CDDP/m suffered corrosion by chlorides in medium, yet the optically active micelles with α-helix bundles kept the micelle structure for prolonged time, with slowly releasing unimers and dimers from the surface of the bundled core in an erosion-like process, as verified by ultracentrifugation analysis. This is in sharp contrast with the abrupt disintegration of CDDP/m from PEG-P(D,LGlu) without secondary structures. The tailored assembly in the core of the polymeric micelles through regular arrangement of constituting segments is key to overcome their undesirable disintegration in bloodstream, thereby achieving efficient delivery of loaded drugs into target tissues.

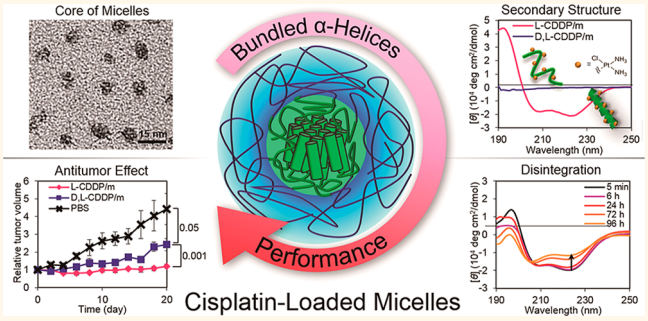


**KEYWORDS:** targeted cancer therapy · drug delivery systems · polymeric micelle · cisplatin · poly(glutamic acid) · secondary structure · α-helix

Supramolecular nanoarchitectures built through self-assembly of amphiphilic block copolymers have high potential for biomedical application due to their capability of tailoring their structural and functional features by engineering the assembly mode of the building blocks.[1−6] Although precise control of the structure and function of nanoassemblies is still challenging, in nature, biological macromolecules, such as polypeptides, present well-defined spatial arrangements constructed *via* hierarchical assembly from secondary structures, such as α-helix and β-sheet, to higher-order structures, which uniquely provide them with sophisticated biological functions.

* Address correspondence to kataoka@bmw.t.u-tokyo.ac.jp, nishiyama@res.titech.ac.jp.

Received for review January 25, 2014 and accepted June 10, 2014.

**Published online June 10, 2014**
10.1021/nn500498t

Taking advantage of these biological macromolecules, there have been many approaches of utilizing polypeptide-based block copolymers to prepare supramolecular nanoassemblies with targeted structural and biological properties.[7−10] Because of the ability of polypeptides to form higher-order structures, the polypeptide segments of these block copolymers allow tuning the spatial arrangements,[7,8] which can determine the structural stability and function of the nanoassemblies.

Among promising nanoassemblies, polymeric micelles constructed from poly(ethylene glycol) (PEG)-polypeptide block copolymers have shown high potential as targeted nanomedicines.[10,11] The core−shell nanostructure of polymeric micelles is a substantial advantage for delivering bioactive payloads to diseased tissues, as they can incorporate a broad variety of molecules within their core,[11] while the PEG shell protects the cargo and prolongs the half-life of the micelles during blood circulation by avoiding interaction with the surrounding biological environments.[12] Polymeric micelles prepared from PEG-*b*-poly(aspartic acid) and PEG-*b*-poly(glutamic acid) copolymers, incorporating antitumor drugs chemically conjugated to the polypeptide blocks, have been used as drug delivery systems, showing high stability and long circulation in the bloodstream,[13,14] and selectively accumulating in tumor tissues.[13−15] Thus, several polymeric micelles incorporating antitumor drugs are currently under human clinical evaluations, showing enhanced antitumor efficacy and reduced side effects.[13−16] The successful pharmaceutical properties of these polymeric micelles could be related to the structure of their core, which consists of the polypeptide blocks. As polypeptides consisting of monomer units with identical configuration have tendency to adopt secondary structures in their backbones, the assembly of the polymeric micelles may be built from secondary structures in a similar way as proteins, in turn modulating the physicochemical properties of the polymeric micelles, such as their critical association concentration, association number, size distribution and stability,[7,8] which may directly affect their biological performance. While research focusing on developing drug delivery systems has been most often directed at the chemical modification of polymer chains by introducing hydrophobic groups, polar groups or cross-linking for improving the stability of the carriers,[1,3,10] little attention has been paid on the effect of secondary structures of polymer chains on the drug delivery performance of nanomedicines.

In this study, we examined the secondary and higher order structures in cisplatin-loaded polymeric micelles (CDDP/m) as successful carriers, which are being evaluated in phase III human clinical trials in several countries,[16,17] to clarify the effect of these structures in the biological performance of polymeric micelles. CDDP/m are self-assembled through the coordination bonds between carboxylate moieties of PEG-*b*-poly(L-glutamic acid) (PEG-*b*-P(L-Glu)) copolymer and cisplatin in water, which cancels the negative charges of the carboxylates and increases the hydrophobicity of the poly(L-glutamic acid) (P(L-Glu)) blocks. Thus, the core of CDDP/m is composed of cisplatin-conjugated P(Glu) blocks, which may adopt secondary structures *via* hydrogen bonds between backbone amides. To clarify the significance of the secondary structure in the CDDP/m, three types of PEG-*b*-P(Glu) with different optical activity, *i.e.*, PEG-*b*-Poly(L-glutamic acid) (L-Polymer) and PEG-*b*-poly(D-glutamic acid) (D-Polymer), which can form regular secondary structures, and PEG-*b*-poly(D,L-glutamic acid) (D,L-Polymer), which adopts mainly random conformation, were synthesized and used for preparing a series of CDDP/m (L-, D- and D,L-CDDP/m, respectively). Thus, by focusing on the differences in the secondary structure of the P(Glu) block, the formation process, the structural characteristics, and the physicochemical properties of the series of CDDP/m, as well as their ability as tumor-targeted drug carriers, were comprehensively examined to illustrate the significance of tailoring secondary structures as a novel and universal strategy for constructing supramolecular nanomedicines with improved drug delivery performance.

## RESULTS AND DISCUSSION

**Synthesis and Characterization of Polymers.** *N*-Carboxyanhydride of $\gamma$-benzyl L-glutamate (NCA-BLG) and *N*-carboxyanhydride of $\gamma$-benzyl D-glutamate (NCA-BDG) were polymerized from the $\omega$-$NH_2$ group of PEG *via* ring-opening polymerization to afford optically pure PEG-*b*-poly($\gamma$-benzyl L-glutamate) (PEG-*b*-PBLG) and PEG-*b*-poly($\gamma$-benzyl D-glutamate) (PEG-*b*-PBDG), respectively. Similarly, PEG-*b*-poly($\gamma$-benzyl D,L-glutamate) (PEG-*b*-PBDLG) was synthesized from the equimolar mixture of NCA-BLG and NCA-BDG monomers. Gel permeation chromatography of these polymers showed the formation of narrowly distributed block copolymers ($M_w/M_n$ = 1.03, 1.03, and 1.07 for PEG-*b*-PBLG, PEG-*b*-PBDG and PEG-*b*-PBDLG, respectively) (Figure S1, Supporting Information). Benzyl groups were deprotected with 5-fold molar mass of NaOH to the benzyl ester units *via* alkali hydrolysis. Complete deprotection was confirmed by the absence of the peaks of benzyl group on the $^1$H NMR spectra (Figure S2, Supporting Information). By comparing the integration of the methylene protons in the PEG block with that of $\alpha$, $\beta$ and $\gamma$ protons in the P(Glu) block, the degree of polymerization of the P(Glu) block was calculated to be 40 for every polymer.

To confirm the ability of P(Glu) block of L- and D-Polymer to adopt regular secondary structure, circular dichroism (CD) spectra of these block copolymers were recorded at acidic condition, as homo poly(L-glutamic acid) is known to adopt $\alpha$-helix at acidic pH below the

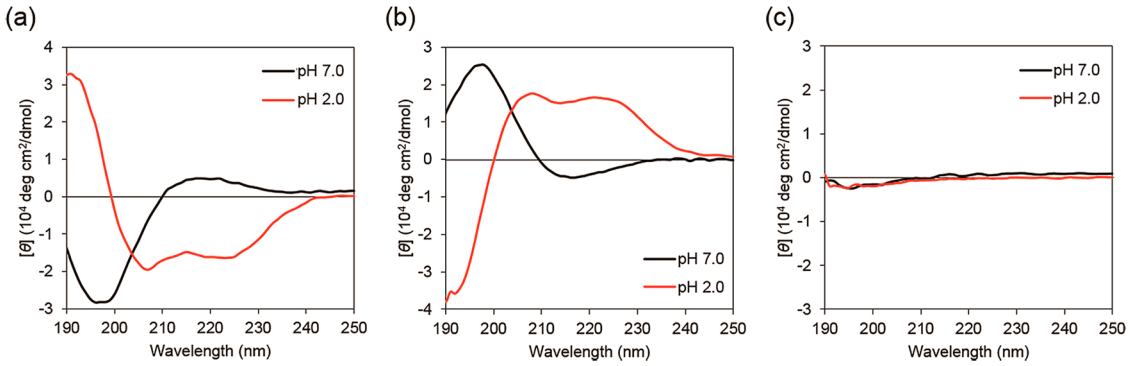


**Figure 1. Circular dichroism spectra of (a) L-Polymer, (b) D-Polymer, and (c) D,L-Polymer in aqueous solution at pH 7.0 (black) and 2.0 (red).**

p$K_a$ of the carboxylic moieties.[18] The CD spectra of L- and D-Polymer showed double minima and double maxima at 208 and 222 nm at pH 2.0, respectively, indicating the formation of right-handed α-helix in L-Polymer and left-handed α-helix in D-Polymer, while both polymers presented random coil conformation at neutral condition (Figure 1a,b). Conversely, CD signal from D,L-Polymer was not detectable because the signals were canceled due to the racemic composition (Figure 1c). Moreover, $^1$H NMR spectra of the polymers in $D_2O$ were recorded to confirm their secondary structure at pD 2.0 (Figure S3, Supporting Information), as it was reported that the peak derived from $C_\alpha$ protons of the P(Glu) blocks shifts to higher magnetic field upon α-helical formation.[19] At pD 2.0, the peak of $C_\alpha$ protons of the L-Polymer and D-Polymer split into two peaks, which indicates the presence of both α-helix and random conformation, while that of D,L-Polymer remained unchanged, suggesting random conformation (Figure S3, Supporting Information).[19]

**Formation Process of Cisplatin-Loaded Micelles (CDDP/m).** As we reported previously, the complexation of cisplatin with the carboxylate moieties of L-Polymer in aqueous solution leads to the formation of L-CDDP/m.[20] Herein, to examine the ability of the series of PEG-*b*-P(Glu) to form CDDP/m, and to obtain insights on the resulting structure, the formation process of these micelles was followed by spectrometry.

First, the assembly process of the block copolymers was examined by static light scattering (SLS). Scattered light intensity of the cisplatin/PEG-*b*-P(Glu) mixture was monitored and converted to excess Rayleigh ratio ($\Delta R(90°)$), which is proportional to the weight-averaged molecular weight and concentration of solutes.[21] A significant increase in $\Delta R(90°)$ value was observed for every formulation (Figure 2a), indicating that all types of the block copolymers were able to assemble into micelles by the conjugation of cisplatin regardless of their configuration in the P(Glu) blocks. Noteworthy is that the solutions of L- and D-Polymer showed an accelerated increase in the $\Delta R(90°)$ value after 5 h, while the $\Delta R(90°)$ value for D,L-Polymer solution increased linearly for 48 h (Figure 2a, inset).

To investigate the cause of this difference, the reaction of cisplatin with the series of PEG-*b*-P(Glu) was examined by UV spectrometry, as it was reported that square planar platinum complexes display UV absorbance in the 250 nm region due to d-d electronic transitions, and their wavelength varies with the type of the coordinating ligands.[22] According to our previous study, the reaction of cisplatin with the carboxylate moieties of PEG-*b*-poly(α,β-aspartic acid) gives rise to the UV absorbance at 249 nm.[23] Thus, we followed the complexation of cisplatin with the series of PEG-*b*-P(Glu) in water by measuring the UV absorbance at 249 nm over time (Figures 2b and S4, Supporting Information). Within the initial 24 h, every solution showed comparable increase in the absorbance, which indicated that the reaction of cisplatin proceeded similarly and, therefore, that there were other factors which caused the accelerated increase of $\Delta R(90°)$ value after 5 h for L- and D-Polymer (Figure 2a).

Conjugation of cisplatin to the negatively charged carboxylates on the P(Glu) blocks could lead to the cancellation of their electrostatic repulsion, which may induce the formation of secondary structures in the P(Glu) backbones. Thus, the CD spectra of the aqueous solution of cisplatin/block copolymer mixtures were followed to monitor the induction of secondary structure in the P(Glu) blocks. For L-Polymer, the CD spectrum showed random coil structure at the beginning, followed by the gradual decrease in the mean residue ellipticity at 208 and 222 nm ($[\theta]_{208}$ and $[\theta]_{222}$, respectively) (Figure 2c), indicating the formation of right-handed α-helix. The time course of the $[\theta]_{222}$ value, which is proportional to the α-helical content, showed relatively fast formation of α-helix until 5 h followed by its gradual development until 24 h (Figure 2d). D-Polymer showed comparable increase of the $[\theta]_{222}$ value with L-Polymer, but on the opposite direction of the signal (Figure 2d), indicating the formation of left-handed α-helix at a rate similar to L-Polymer. In addition, for both L-Polymer and D-Polymer,

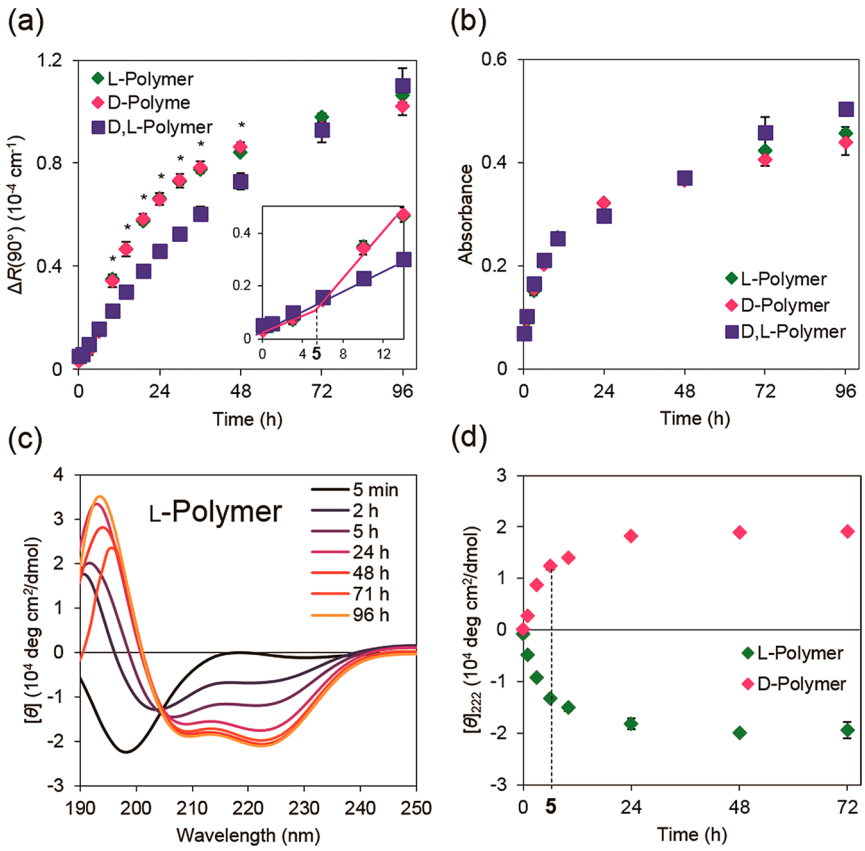


**Figure 2. Formation process of cisplatin-loaded micelles (CDDP/m) prepared from a series of PEG-*b*-P(Glu) (L-Polymer, D-Polymer and D,L-Polymer). (a) Variation in excess Rayleigh ratio ($\Delta R(90°)$) over time. The inset in (a) shows the magnification for the initial 14 h. Data are the mean ± SD, $n = 3$. *$P < 0.005$. (b) Variation in UV absorbance at 249 nm over time. Data are the mean ± SD, $n = 3$. (c,d) Variation over time in (c) circular dichroism spectra and (d) mean residue ellipticity at 222 nm ($[\theta]_{222}$). Data are the mean ± SD, $n = 3$. All the data were collected during the reaction of cisplatin with a series of PEG-*b*-P(Glu) in aqueous solution ([Pt] = [Glu] = 5 mM) at 37 °C.**

approximately half of the whole process of α-helix formation proceeded by 5 h (Figure 2d), which corresponded with the starting point of the accelerated increase in $\Delta R(90°)$ value (Figure 2a, inset). As racemic D,L-Polymer did not show such rapid increase in the $\Delta R(90°)$ value (Figure 2a, inset), the formation of α-helix in the P(Glu) blocks may assist the assembly of L- and D-Polymer into micelles, probably due to the exclusion of water molecules from the amide groups of the P(Glu) backbones.[24] Moreover, the time courses of the $[\theta]_{222}$ value observed for L- and D-Polymer were consistent with the increase in the UV absorbance at 249 nm (Figure 2b,d), implying the crucial role of cisplatin in the induction of α-helix. As the hydrolysis of cisplatin liberates protons, there may be a possibility of inducing α-helix due to pH drop.[25] Thus, to estimate this possibility, the α-helix content in L-Polymer without cisplatin was evaluated by CD spectrometry at pH 5.2, which corresponded to the pH of the cisplatin/polymer solution after 120 h. The spectrum showed the major presence of random conformation along with a minor contribution from α-helix, as observed in the 2.8 times less magnitude in the $[\theta]_{222}$ value than the spectrum of L-Polymer/cisplatin solution after 120 h reaction (Figure S5, Supporting Information). Accordingly, during the formation of CDDP/m, α-helix was induced in L-Polymer by cisplatin complexation of the flanking carboxylates in the P(Glu) block with minor contribution from the protonation of the carboxylates.

**Morphology and Molecular Weight of Micelles.** The series of cisplatin/PEG-*b*-P(Glu) mixture reacted for 120 h were purified through ultrafiltration to obtain pure L-, D- and D,L-CDDP/m for studying their structural characteristics. Cumulant analysis of dynamic light scattering (DLS) revealed that every type of micelles has a comparable hydrodynamic diameter of approximately 25 nm with low polydispersity index (Table 1). Moreover, under transmission electron microscopy (TEM), the core of micelles was observed by positive-staining with uranyl acetate, as their PEG shell cannot be observed due to the lower electron density compared to the stained core. The obtained TEM pictures showed the nearly spherical and monodispersed core of the micelles with an average diameter of 9.3−9.4 nm (Figure 3 and Table 1). It is worth noticing that the distribution of the core diameter of D,L-CDDP/m was relatively broader than that of L- and D-CDDP/m (Figure 3d−f).

**TABLE 1. Structural Characteristics of Cisplatin-Loaded Micelles (CDDP/m)**

| | | | | | yield[e] (%) | | | |
|---|---|---|---|---|---|---|---|---|
| micelle | $d_{micelle}$[a] (nm) | PdI[b] | $d_{core}$[c] (nm) | [Pt]/[Glu][d] (mol/mol) | Pt | polymer | $N$[f] | % helix[g] |
| L-CDDP/m | 24 ± 1 | 0.062 ± 0.01 | 9.3 ± 1.4 | 0.69 ± 0.03 | 31 ± 2 | 45 ± 2 | 18 | 67 ± 3 |
| D-CDDP/m | 24 ± 1 | 0.082 ± 0.02 | 9.3 ± 1.6 | 0.70 ± 0.07 | 34 ± 3 | 48 ± 1 | 18 | 65 ± 5 |
| D,L-CDDP/m | 25 ± 1 | 0.11 ± 0.03 | 9.4 ± 2.0 | 0.92 ± 0.06 | 20 ± 1 | 22 ± 1 | 23 | — |

[a] Weight-averaged hydrodynamic diameter measured by dynamic light scattering (DLS) at 25 °C. Data are the mean ± SD; $n = 3$. [b] Polydispersity index (PdI) measured by DLS represented by an equation: $PdI = \mu_2/\Gamma^2$, where $\mu_2$ is numerical constant at the second cumulant, and $\Gamma$ is the average line width of an electric field autocorrelation function. Data are the mean ± SD; $n = 3$. [c] Diameter of core of micelles measured from the image obtained by transmission electron microscopy ($n = 200$). [d] Molar ratio of platinum atoms to glutamate residues in micelles. Data are the mean ± SD; $n = 3$. [e] Yield of micelles based on either platinum or polymer. Data are the mean ± SD; $n = 3$. [f] Number of polymers associated in a micelle. [g] Percent of α-helix in P(Glu) blocks calculated by the following equation: % helix = $([\theta]_{222} - [\theta]_{222,R})/([\theta]_{222,H} - [\theta]_{222,R})$ (where $[\theta]_{222}$ is the measured mean residue ellipticity of the micelles at 25 °C, $[\theta]_{222,R}$ and $[\theta]_{222,H}$ are the mean residue ellipticity of poly(glutamic acid) at 222 nm with 100% random and 100% helix, respectively.)

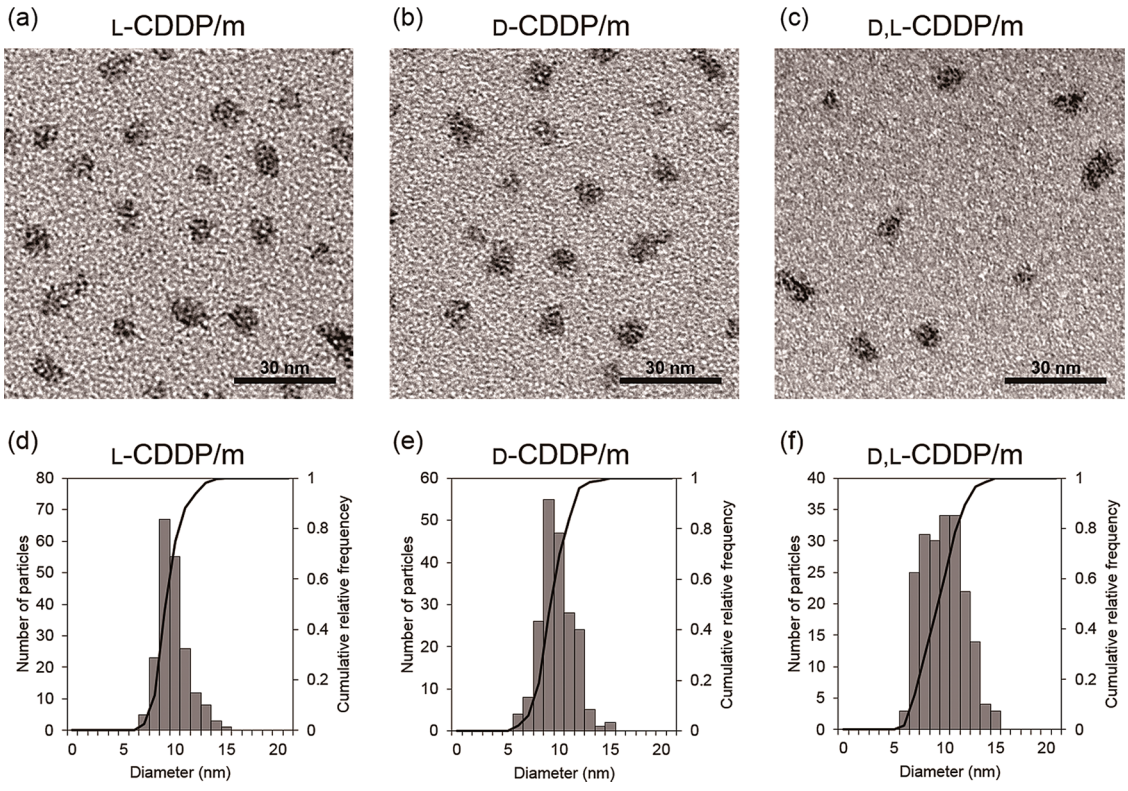


**Figure 3. Core morphology of a series of cisplatin-loaded micelles (CDDP/m) observed by transmission electron microscopy (TEM). Upper panels show positively stained TEM pictures of (a) L-CDDP/m, (b) D-CDDP/m and (c) D,L-CDDP/m. Lower panels show the number-based distribution of the core diameter of (d) L-CDDP/m, (e) D-CDDP/m and (f) D,L-CDDP/m calculated from the corresponding TEM pictures. The cores of the micelles were stained with 2% uranyl acetate. Data are $n$ = 200.**

This slight difference in the distribution of the core diameter of the micelles could be sensitively reflected on the distribution of their molecular weight, which can be estimated by the sedimentation velocity (SV) method of analytical ultracentrifugation. The SV method is widely used to estimate the distribution of sedimentation coefficient of biological polymers by fitting the measured time variation of the sedimentation boundary to the equation of motion for sedimentation phenomena, that is, the Lamm equation.[26] Thereafter, the sedimentation coefficient can be converted to molecular weight by using their partial specific volume ($\bar{v}$), which is the partial derivative of the volume with respect to the mass. In our study, first, the $\bar{v}$ values of the micelles were determined from the linear regression of a density-concentration profile of micelles (Table 2). The smaller $\bar{v}$ values obtained for D,L-CDDP/m may be attributed to the higher loading of cisplatin for these micelles than for L- and D-CDDP/m (Table 1). The observed time variation of the sedimentation boundary was successfully fitted to the Lamm equation and provided the weight- and number-averaged molecular weight of the micelles ($M_w$ and $M_n$, respectively) (Table 2). Accordingly, L- and D-CDDP/m had similar low polydispersity in molecular weight ($M_w/M_n$), which was lower than D,L-CDDP/m, as listed in

Table 2. These results are consistent with the narrower distribution of the core diameter for L- and D-CDDP/m than for D,L-CDDP/m (Figure 3d–f), suggesting that uniform micelles were obtained when the P(Glu) blocks adopted α-helical structure. The validity of these SV results was further confirmed by the similar $M_w$ values determined by sedimentation equilibrium method (Table 2), which is conventionally applied for the determination of weight-averaged molecular weight of polymers.

The amount of cisplatin and polymers incorporated in the micelles was examined by inductively coupled plasma mass spectrometry (ICP-MS) and by measuring the weight of dried micelles, respectively, and presented as the molar ratio of cisplatin to the glutamate residues ([Pt]/[Glu]) in Table 1. L- and D-CDDP/m showed comparable [Pt]/[Glu] values, which were smaller than the value for D,L-CDDP/m. As D,L-CDDP/m formed without additional hydrophobicity by α-helix formation (Figure 2a), further conjugation of cisplatin may be necessary for D,L-Polymer to associate into micelles. Therefore, only the polymers with relatively high [Pt]/[Glu] value could associate into micelles, as indicated by the relatively low yield of D,L-CDDP/m (Table 1), *i.e.*, the percentage of the amount of cisplatin or polymers incorporated in the micelles compared to the fed amount. In addition, by dividing the $M_w$ of the micelles by the corresponding molecular weight of polymer-cisplatin conjugates, which was derived from the molecular weight of the polymers and the [Pt]/[Glu] values (Table 1), the weight-averaged association number of polymers in a single micelle, *N*, was calculated and listed in Table 1 for further discussion of the structure of the micelles.

**TABLE 2. Partial Specific Volume and Molecular Weight of a Series of Cisplatin-Loaded Micelles (CDDP/m)**

| | | velocity[b] | | | equilibrium[c] |
|---|---|---|---|---|---|
| micelle | $\bar{v}$[a] (cm²/g) | $M_w$ | $M_n$ | $M_w/M_n$ | $M_w$ |
| L-CDDP/m | 0.608 | $4.4 \times 10^5$ | $3.4 \times 10^5$ | 1.3 | $4.3 \times 10^5$ |
| D-CDDP/m | 0.610 | $4.4 \times 10^5$ | $3.4 \times 10^5$ | 1.3 | $4.3 \times 10^5$ |
| D,L-CDDP/m | 0.577 | $6.3 \times 10^5$ | $3.2 \times 10^5$ | 2.0 | $6.5 \times 10^5$ |

[a] Partial specific volume of micelles determined by densimetry. [b] Weight-averaged and number-averaged molecular weight ($M_w$ and $M_n$, respectively) of micelles estimated by sedimentation velocity method of analytical ultracentrifugation. [c] Weight-averaged molecular weight of micelles estimated by sedimentation equilibrium method of analytical ultracentrifugation.

**Nanostructure in the Core of Micelles.** As mentioned above, right- and left-handed α-helix were induced in the P(Glu) blocks during the formation of L- and D-CDDP/m, respectively (Figure 2c,d). Herein, the arrangement of these secondary structures in the core of these CDDP/m was investigated. First, the geometric feature of α-helices in the P(Glu) block of L- and D-CDDP/m was quantitatively analyzed by CD spectrometry. CD spectra of L- and D-CDDP/m presented similar magnitudes on opposite sides, indicating optically symmetric conformations of the P(Glu) blocks (Figure 4a). The $[\theta]_{222}$ value revealed that the α-helical content of the P(Glu) blocks was approximately 65% for both micelles (Table 1), showing that 26 residues out of 40 residues of a P(Glu) block adopt α-helix on average. Because α-helix has a translation of 0.15 nm per residue along the axis,[27] and molecular modeling indicated that the diameter of the α-helix of the cisplatin-conjugated P(Glu) is 1.5 nm (Figure S6, Supporting Information), we can regard the α-helix as a cylinder with 3.9 nm (= 0.15 nm × 26) of height and 1.5 nm of diameter.

Second, aqueous solution of L-CDDP/m was further examined by small-angle X-ray scattering (SAXS) to obtain insights on the arrangement of cylindrical α-helices in the core of the micelles. SAXS profiles of L-CDDP/m presented three distinct peaks around $q$ = 0.2, 0.5, and 5 nm$^{-1}$ (Peak 1, 2 and 3, respectively)

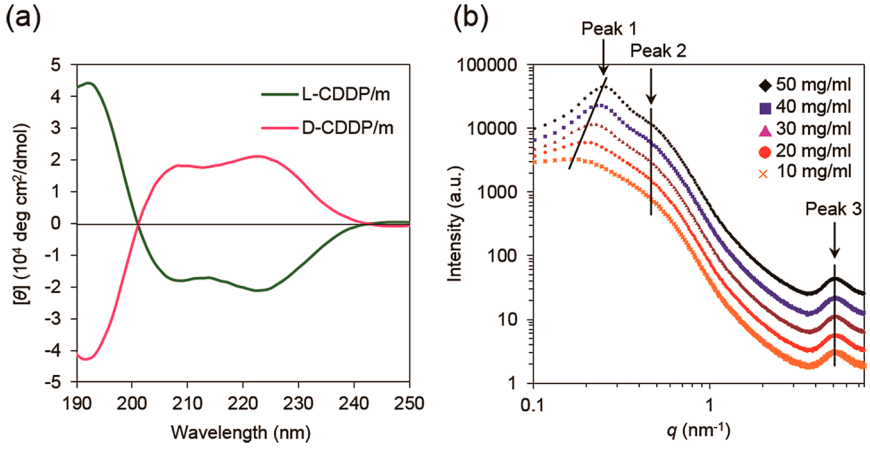


**Figure 4. Secondary structures and their assembly in the core of cisplatin-loaded micelles (CDDP/m). (a) Circular dichroism spectra of L-CDDP/m and D-CDDP/m at 25 °C. (b) Small angle X-ray scattering (SAXS) profiles of L-CDDP/m at different concentration. The solid black lines indicate the positions of the peak tops. The profiles were arbitrarily shifted along the vertical axis.**

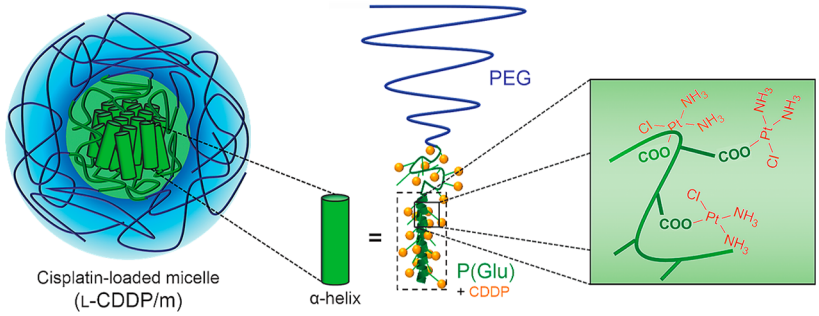


**Scheme 1. Proposed hierarchical structure of cisplatin-loaded micelles (CDDP/m) prepared through the self-assembly of poly(ethylene glycol)-*b*-poly(L-glutamic acid) [PEG-*b*-P(Glu)] after polymer-metal complex formation with cisplatin. The core of the micelles is composed of 18 P(Glu) blocks, which form associated α-helix bundles, being surrounded by a PEG shell. The carboxylates in the P(Glu) blocks coordinate with cisplatin.**

(Figure 4b), which were resolved by computer-assisted peak fitting (Table S1, Supporting Information). Second derivative spectra of the SAXS profiles visually confirmed the presence of Peak 2 (Figure S7, Supporting Information). Peak 1, which gives a spacing of approximately 30 nm (Table S1, Supporting Information), shifted to higher $q$ direction as the concentration of the micelles increased, probably due to intermicellar interference caused by high concentration (>10 mg/mL). Conversely, Peak 2 and 3, which correspond to a spacing of 13.5 and 1.24 nm, respectively, did not shift with concentration (Table S1, Supporting Information) and, thus, can originate from the structure of the micelles. As a form factor of core−shell particle with corresponding size to L-CDDP/m gives shoulder around $q$ = 0.5 $nm^{-1}$ (Figure S8, Supporting Information), Peak 2 is probably derived from the core−shell structure of the micelles. In contrast, the significantly small length scale of Peak 3 indicates that Peak 3 may be derived from the internal structure of the core of the micelles. As indicated in the micelle formation study, α-helices provide the P(Glu) segments with increased hydrophobicity, which may allow the α-helical P(Glu) segments to localize at the deep core region of the micelles for avoiding the unfavorable interaction with surrounding water. Thereafter, due to the inherent tendency of cylindrical α-helices to laterally align with each other,[28−30] these α-helical P(Glu) segments may be arranged in a bundle structure, which is supported by previous SAXS observations on multihelix bundles showing peaks comparable to Peak 3 due to interhelical interference.[31] Moreover, if the closest arrangement of α-helices is assumed, Peak 3 may be produced by the diffraction plane of this hexagonal lattice,[32] giving an interhelical distance of 1.43 nm (= 1.24 nm × $2/\sqrt{3}$) (Scheme S1, Supporting Information), which is possible because the diameter of the cisplatin-conjugated α-helix of P(L-Glu) is 1.5 nm. In addition, from the CD spectrum of L-CDDP/m, the lateral alignment of α-helices was further supported by the ratio of the mean residue ellipticity at 222 nm and at 208 nm ($[\theta]_{222}/[\theta]_{208}$ = 1.1) (Figure 4a), which indicates the presence of lateral interaction of α-helices when the value is close to or larger than 1.0.[33] All these results support that α-helices are arranged in a bundle structure in the core of L-CDDP/m.

By summarizing the above-mentioned structural results, the following hierarchical assembly for L-CDDP/m was proposed: initially, the conjugation of cisplatin to the carboxylate groups of the P(Glu) blocks increased hydrophobicity of the segment, followed by the additional increase in hydrophobicity due to the formation of α-helix, probably due to the exclusion of water molecules from the backbone amides,[24] leading to the self-assembly of the cisplatin conjugated block copolymers into core−shell polymeric micelles with uniform size (Figures 2 and 3 and Table 1); upon the assembly of the micelles, the hydrophobicity of α-helices and their tendency to align laterally[28−30] may promote the formation of an α-helix bundle in the deep core region of the micelles to avoid unfavorable interaction with surrounding water. Thus, flexible P(Glu) segments in random conformation are placed between the α-helical P(Glu) bundle and the hydrophilic PEG chains (Scheme S2a, Supporting Information), allowing spherical shape of the micelle core (Figure 3a). Therefore, taking into consideration that the average association number of a micelle was 18 (Table 1), we propose the total structure of L-CDDP/m in Scheme 1. The rationality of the proposed model was further discussed in Scheme S2 (Supporting Information) from the viewpoint of its structural dimension.

**Disintegration of Micelles in Physiological Conditions.** Polymeric micelles as tumor-targeted drug delivery systems require physicochemical properties capable of maintaining the micellar structure in blood and preventing release of the loaded drugs until reaching the tumor tissues. As reported previously, CDDP/m show sustained disintegration process in physiological condition, which initiates with the release of cisplatin by the reaction of chloride ions with the cisplatin complexed to the carboxylates in the P(Glu) blocks of PEG-*b*-P(Glu), followed by the disassembly of the micellar structure due to the increased electrostatic

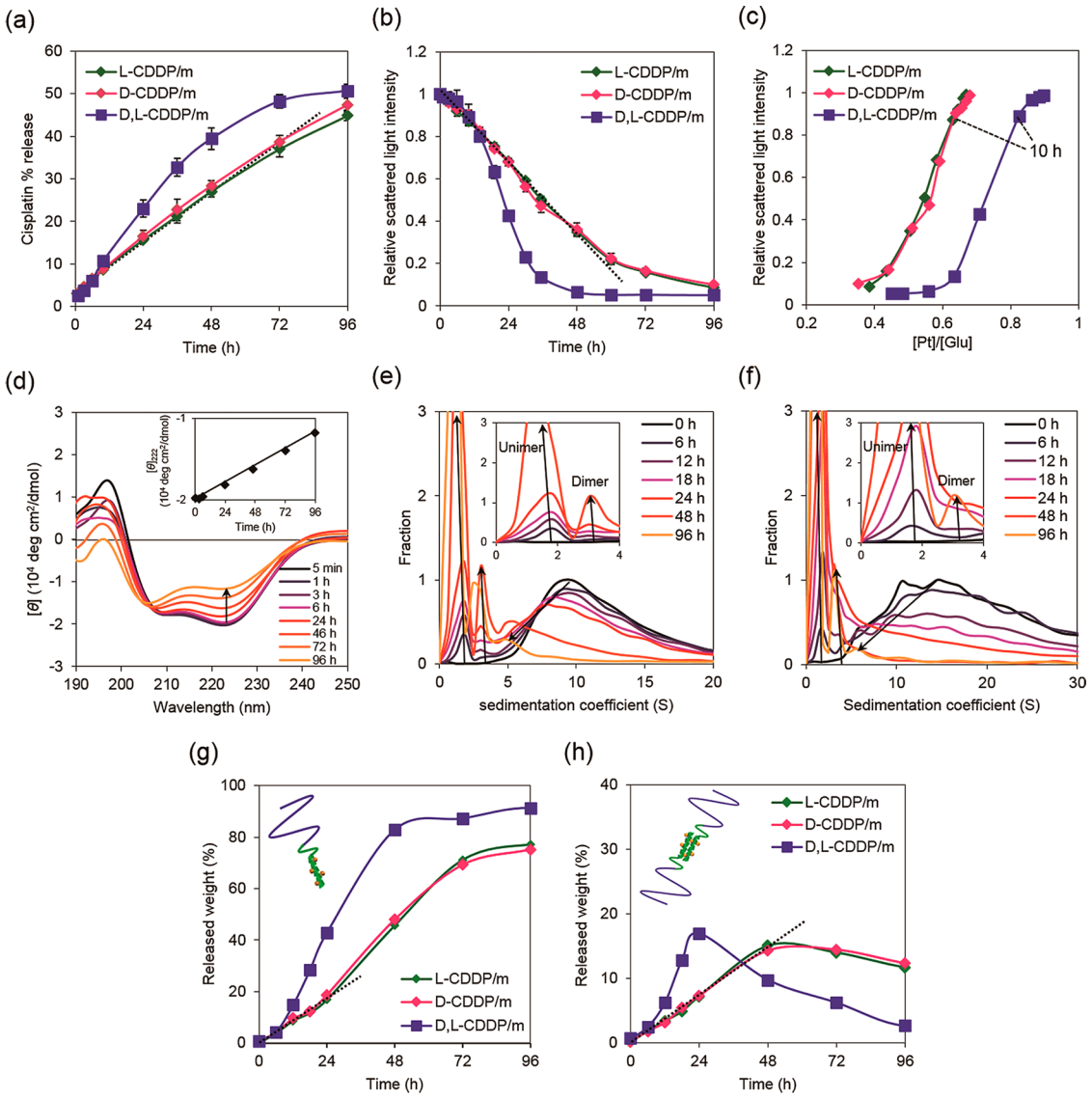


**Figure 5. Disintegration of the series of cisplatin-loaded micelles (CDDP/m) in physiological condition (10 mM phosphate buffer solution containing 150 mM NaCl (pH 7.4) at 37 °C). (a) Release profiles of free cisplatin. Data are the mean ± SD, $n = 3$. (b) Variation in relative scattered light intensity at a detection angle of 90° normalized to the initial value. Data are the mean ± SD, $n = 3$. (c) Correlation between relative scattered light intensity and fraction of cisplatin-conjugated glutamate residues ([Pt]/[Glu]) during disintegration process. (d) Variation in CD spectra of L-CDDP/m. The inset shows variation in mean residue ellipticity at 222 nm ($[\theta]_{222}$). (e,f) Variation in distribution of sedimentation coefficient of (e) L-CDDP/m and (f) D,L-CDDP/m analyzed by sedimentation velocity method of analytical ultracentrifugation. The insets in (e) and (f) are the magnification at the region of small sedimentation coefficient for the first 48 h. (g,h) Discharge of (g) unimers and (h) dimers from the micelles.**

repulsion and decreased hydrophobicity.[20] Herein, to reveal the roles of α-helix bundles in the core of CDDP/m in this disintegration process, the drug release and disassembly process in physiological conditions, *i.e.*, phosphate buffered saline containing 150 mM NaCl (PBS; pH 7.4) at 37 °C, were investigated for the series of CDDP/m.

The release of cisplatin from CDDP/m was examined by dialyzing the micelles against PBS, followed by the quantification of the released cisplatin by ICP-MS. As the dialysis membrane has a molecular weight cutoff size of 1000 Da, which is much smaller than the molecular weight of polymers, only free cisplatin was followed here. L- and D-CDDP/m showed similar linear increase of released cisplatin in a sustained fashion, while D,L-CDDP/m showed relatively accelerated and faster release than the other micelles after 10 h (Figure 5a). As the release of cisplatin is expected to destabilize the micelle structure, the disassembly of CDDP/m in similar conditions was monitored by following the scattered light intensity, which was normalized to the initial intensity. For L- and D-CDDP/m, the scattered light intensity gradually decreased over 96 h, whereas D,L-CDDP/m showed a progressive decrease in the scattered light intensity after 10 h (Figure 5b). The contrasting profiles of the intensity-time curves suggest that the process governing the disassembly of L- and D-CDDP/m may be different from that of D,L-CDDP/m. Moreover, to compare

the structural stability of the series of CDDP/m, the relative scattered light intensity obtained at each time point in Figure 5b was plotted against the fraction of cisplatin-complexed glutamate residues ([Pt]/[Glu]) at the corresponding time (Figure 5c), which was calculated from the initial [Pt]/[Glu] ratio and the amount of released cisplatin (Table 1 and Figure 5a). The profiles in Figure 5c showed that D,L-CDDP/m needed higher amount of cisplatin conjugated to the P(Glu) blocks than L- and D-CDDP/m for maintaining their assembled structure, indicating the higher structural stability of L- and D-CDDP/m. From these results, it is reasonable to conclude that the process of disintegration and structural stability of CDDP/m is regulated by the packaging state of P(Glu) strands in the core of the micelles, as L- and D-CDDP/m have an ordered core structure based on α-helix bundles, which is in complete contrast to the random aggregation of P(Glu) strands in D,L-CDDP/m. Then, to estimate the change in the secondary structure of L-CDDP/m during the disintegration process, CD spectra of L-CDDP/m was monitored under similar conditions. The isodichroic point at 205 nm (Figure 5d), which is indicative of two-state transition, and gradual decrease in the absolute $[\theta]_{222}$ value (Figure 5d, inset) showed that the α-helices in the L-CDDP/m gradually shifted to random conformation in a linear fashion probably due to the increased electrostatic repulsion among the charged carboxylates of the P(L-Glu) blocks accompanying the release of cisplatin. Nevertheless, even after 96 h, the α-helical content in the P(L-Glu) blocks remained higher than 40%, as calculated from the $[\theta]_{222}$ value (Figure 5d, inset). These observations confirmed that a significant amount of α-helices were retained in the P(Glu) blocks during the disintegration process of L-CDDP/m, and suggest a critical role of the α-helix bundles in the disassembly mechanism of the micelles.

To investigate the contribution of the α-helix bundles in the disassembly process of the micelles, the pathway of disassembly was examined in detail by applying the SV method of analytical ultracentrifugation to the micelle solutions collected at defined time points during the disassembly study. The variation in the distribution of the sedimentation coefficient for L- and D,L-CDDP/m showed that two peaks, corresponding to unimer and dimer of cisplatin/polymer conjugates (Table S2, Supporting Information), emerged over time regardless of the configuration of the P(Glu) blocks with a gradual shift of the peak derived from multimolecular assemblies (micelles) toward lower sedimentation coefficient (Figure 5e,f). From these profiles, the weight fraction of the unimers and dimers discharged into the solution was calculated and plotted against time for every micelle formulation (Figure 5g,h). In the final phase after 96 h incubation, even though 90% of the polymers were discharged as unimers and dimers from the micelles, only 45−50% of cisplatin was released as free drug, indicating that half of the total amount of cisplatin was still bound to the discharged unimers and dimers. Moreover, while L- and D-CDDP/m showed a gradual and relatively constant discharge of unimers and dimers over time range of 72 h, there was an accelerated discharge of unimers and dimers from D,L-CDDP/m even after 10 h, which correlated with the starting time point of the progressive decline in scattered light intensity (Figure 5b). According to Figure 5a, approximately 10% of cisplatin was released from D,L-CDDP/m after 10 h, corresponding to a [Pt]/[Glu] ratio of 0.83, the value below which the disassembly of D,L-CDDP/m should be promoted, according to Figure 5c. In addition, D,L-CDDP/m showed increased release of cisplatin from 10 h compared to the other micelles. Therefore, the decrease in the hydrophobicity in the core of D,L-CDDP/m due to the initial cisplatin release until 10 h possibly promoted the penetration of water and chloride ions into deep regions of the core, leading to an accelerated release of cisplatin accompanied by an abrupt disassembly of the micelles (Scheme 2). Conversely, the presence of robust α-helix bundles in the core of L- and D-CDDP/m, which can further stabilize the structure by close association of hydrophobic α-helices, may maintain the hydrophobicity of the interior of the core even after release of cisplatin from the outer layer of the bundled assembly, preventing the penetration of chloride ions into deep core region. As a result, the release of cisplatin and discharge of unimers and dimers could gradually proceed from the outer layer of the core to its interior in an ordered manner (Scheme 2). This erosion-like disintegration process was supported by the long-term constant rate of drug release and disassembly observed for L- and D-CDDP/m in physiological condition (Figure 5a,b,g,h). Consequently, the presence of the α-helical bundles in the core of CDDP/m highly impacted on the disintegration process of the micelles by controlling the release of drugs, the ordered discharge of polymers and the maintenance of micelle structure in physiological conditions for a prolonged period, thus, offering a potent strategy for regulating the biological properties of the micelles as nanomedicines.

**Biodistribution.** Selective delivery of cisplatin to tumor tissues is required for achieving high therapeutic efficacy of CDDP/m with reduced systemic toxicity. This specific tumor accumulation can be achieved by utilizing the enhanced permeability and retention (EPR) effect, which is based on the augmented accumulation of macromolecules in tumor tissues due to the higher permeability of tumor vasculature than normal vasculature, and the retention of these macromolecules in tumors due to the impaired lymphatic drainage.[34] Thus, it is necessary for CDDP/m to present a prolonged blood circulation, while preventing nonspecific distribution to the untargeted sites, for maximizing their accumulation in tumor tissues. Herein, the plasma clearance of the series of CDDP/m in relation to

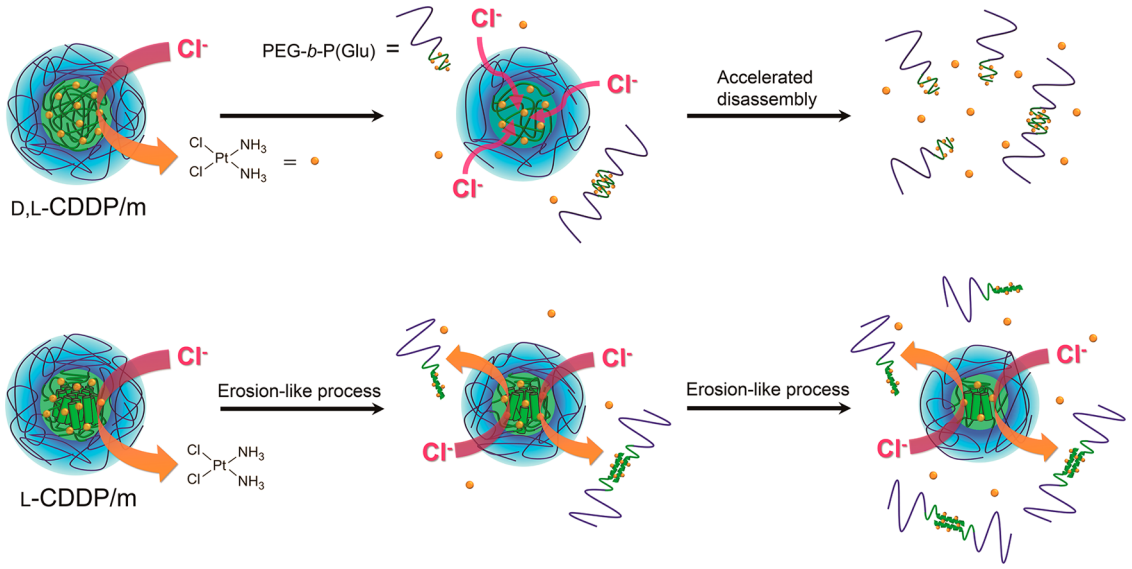


**Scheme 2. Disintegration process of cisplatin-loaded micelles (CDDP/m) prepared from L- and D,L-Polymer. While the disintegration of D,L-CDDP/m without α-helix bundles in the core involved accelerated release of cisplatin and discharge of unimers and dimers, leading to the abrupt disassembly of the micelles, the disintegration of L-CDDP/m proceeded gradually through an erosion-like process, where the release of cisplatin and discharge of unimers and dimers may proceed from the periphery of the bundled core to its interior.**

their distribution to blood cells, organs responsible for the elimination of nanomedicines, *i.e.*, kidney, liver and spleen,[35,36] and solid tumors were investigated. As a model of solid tumor, we used a human pancreatic adenocarcinoma (BxPC3) since the treatment of pancreatic cancer has been aspired because of its high mortality rate, which approximates its incidence rate.[37]

The series of CDDP/m was intravenously injected to mice bearing subcutaneous xenografts of BxPC3, and blood and tissue samples were collected at defined time points. Blood samples were immediately separated to plasma and blood cells by centrifugation. Because the incorporated drug contains a platinum atom, the concentration of the micelles in the biological samples was quantified by ICP-MS. L- and D-CDDP/m showed comparable prolonged blood circulation, as approximately 20 and 3% of the injected dose remained in the plasma at 24 and 48 h, respectively, while D,L-CDDP/m were considerably eliminated from the bloodstream, showing only 0.7 and 0.2% of the injected dose in the plasma at the corresponding time points (Figure 6a). Meanwhile, the distribution of platinum drugs to blood cells was kept significantly low throughout the experiment compared to their concentration in plasma (Figure 6b), confirming that blood cells did not affect the biodistribution of the micelles. Moreover, the accumulation in kidney for all micelles stayed low and slightly decreased over 48 h (Figure 6c), indicating that the kidney clearance was not responsible for the significant drop of D,L-CDDP/m in plasma concentration, Conversely, in liver and spleen, while L- and D-CDDP/m kept their accumulation relatively low over 48 h, D,L-CDDP/m displayed an abrupt increase in the accumulation at 8 h after administration, resulting in much higher platinum levels in liver and spleen than L- and D-CDDP/m (Figure 6d,e). This accumulation of D,L-CDDP/m in liver and spleen corresponded with their decreasing profile in plasma concentration (Figure 6a), that is, from approximately 71% of the injected dose per ml of plasma at 4 h to 29% at 8 h. It has been reported that the uptake of nanocarriers by liver and spleen is associated with the adsorption of proteins on their surface due to impaired stealth efficacy.[36] Because L-, D- and D,L-CDDP/m showed comparable concentration in plasma, liver and spleen during the initial 1−4 h period, it can be inferred that the micelles presented similar intrinsic stealth efficacy in this time period. As the stealth efficacy of block copolymer micelles is considered to be correlated with the PEG density of their shell layer,[38] the PEG density of these micelles was calculated by dividing the association number of the micelles (number of PEG chains on the surface of the core) by the surface area of the micellar core (Table S3, Supporting Information). Thus, we found that D,L-CDDP/m have even higher inherent PEG density than L- or D-CDDP/m, which is apparently inconsistent with an inferior longevity of the former in bloodstream compared to the latter. Alternatively, because the decrease in plasma concentration and the abrupt uptake by liver and spleen of D,L-CDDP/m were observed after 8 h period, it is reasonable to assume that the stealth efficacy of D,L-CDDP/m may dynamically change after their injection into blood compartment. In this regard, it is worth noting the time-dependent variation in the distribution of the sedimentation coefficient of the micelles in PBS (Figure 5e,f). Accordingly, L-CDDP/m maintained the initial peak distribution (10 S at 0 h) over time (Figure 5e), whereas D,L-CDDP/m

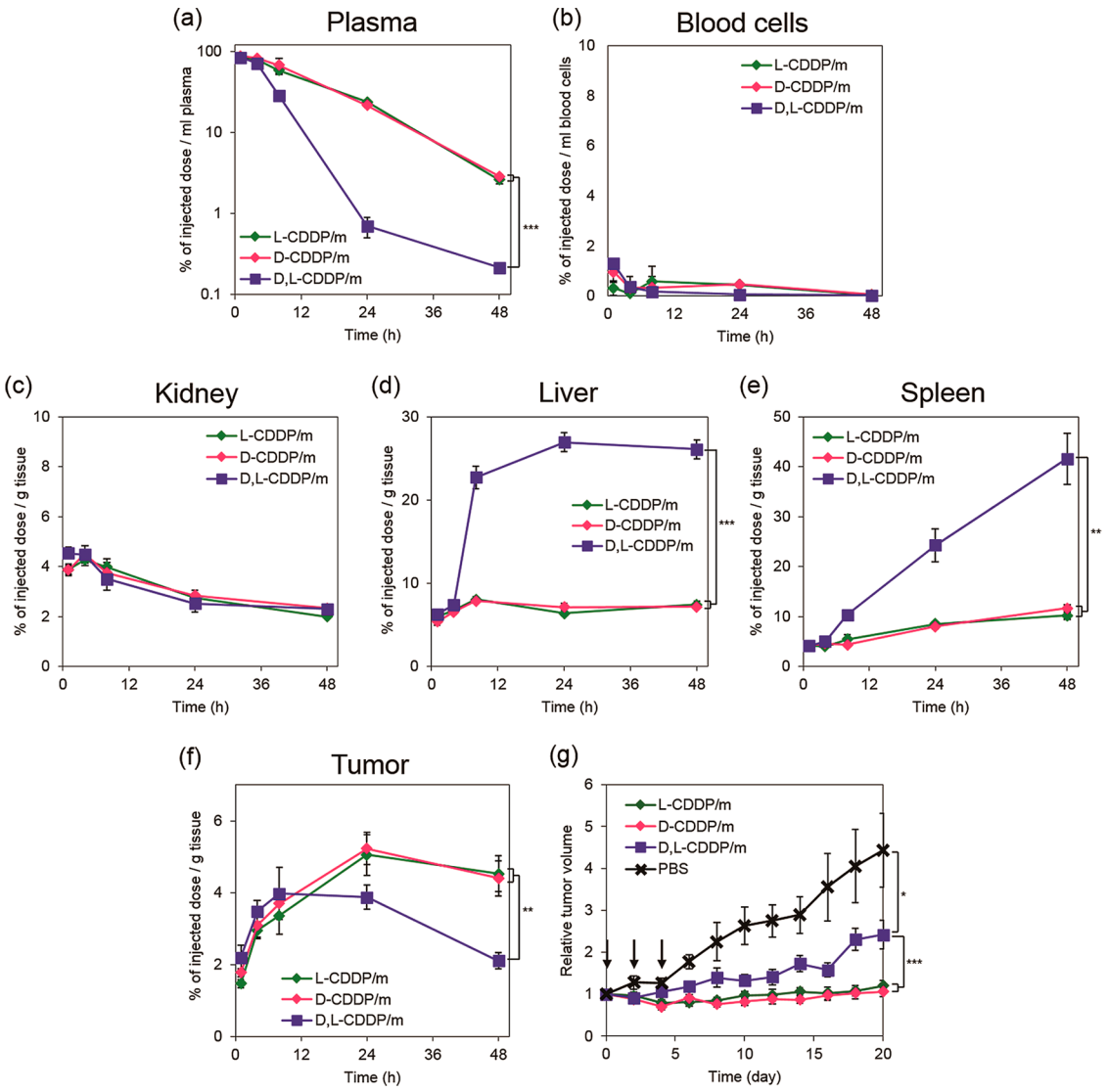


**Figure 6. Biological performance of cisplatin-loaded micelles (CDDP/m) after i.v. administration to BALB/c nu/nu mice bearing a BxPC3 tumor. Time course of the concentration of platinum in (a) plasma and (b) blood cells, and the accumulation of platinum in (c) kidneys, (d) liver, (e) spleen and (f) tumor after i.v. administration of CDDP/m at a dose of 100 $\mu$g/mouse on a cisplatin basis. (g) Antitumor efficacy after three administrations of CDDP/m on days 0, 2, and 4 at a dose of 4 mg/kg on a cisplatin basis. The arrows indicate the day of drug administration. The volume of the tumor was normalized to the initial day (day 0). Data are the mean ± SEM, $n = 5$ [$n = 6$ for (g)]. *$P < 0.05$, **$P < 0.01$, ***$P < 0.001$.**

underwent substantial decrease in the initial fraction (13 S at 0 h) with significant peak broadening during the 6−12 h period (Figure 5f). As the sedimentation coefficient corresponds to the molecular weight, these results demonstrate that the association number of D,L-CDDP/m gained polydispersity during the 6−12 h period, while discharging unimers and dimers as seen in Figure 5g,h. Presumably, this loss of integrity in the structure of D,L-CDDP/m may be responsible for their impaired stealth efficacy during circulation, resulting in their abrupt accumulation in liver and spleen through opsonization (Figure 6d,e). The proposed disintegration process of D,L-CDDP/m was depicted in Scheme 2, where the micelles promptly lose their structural integrity synchronized with discharging unimers and dimers to alter their surface properties. In contrast, L- and D-CDDP/m undergo a well-controlled erosion-like disassembly process with keeping the integrity of the PEG palisade, owing to their ordered-core structure stabilized by α-helix bundles, to exert their stealthiness for prolonged time period.

Finally, to compare the delivery efficiency of the series of CDDP/m to the pancreatic tumor xenografts, the time-course of the concentration of platinum in the tumor was examined and shown in Figure 6f. L- and D-CDDP/m showed a monotonic increase in the cumulative amount of platinum in tumor over 24 h, indicating that the increment of platinum accumulation with time was always positive until 24 h. This observation is consistent with the accumulation mechanism of EPR effect,[34] considering that these micelles still retained

20% of the injected dose in plasma even after 24 h. Conversely, D,L-CDDP/m revealed no increase in platinum accumulation after 8 h, which is consistent with the significant drop in the plasma concentration during this time period. Afterward, the concentration of D,L-CDDP/m considerably decreased at 48 h, whereas L- and D-CDDP/m maintained their accumulation in tumor even at 48 h, achieving 2-fold higher drug levels than D,L-CDDP/m at this time point. If we assume that the micelles disintegrate in tumor tissues in the same manner as in PBS, 90% of D,L-CDDP/m exist as unimers and dimers after 48 h, whereas 50% of L- and D-CDDP/m still exist as micelles (Figure 5g,h). Considering the faster diffusion rate of unimers and dimers than high-molecular weight micelles, it is reasonable to assume that the faster dissociation of D,L-CDDP/m into unimer/dimer than L- and D-CDDP/m may result in their lower retention in tumor tissues. Moreover, the prolonged retention of L- and D-CDDP/m in tumor may be advantageous for tumor therapy, as they can release active cisplatin at the tumor site for prolonged time. From these biodistribution results, the enhanced stability and erosion-like disassembly process of L- and D-CDDP/m were clearly advantageous for extending blood circulation, preventing nonspecific distribution, and achieving high and prolonged accumulation in tumor tissues.

**Antitumor Efficacy.** The elevated accumulation and prolonged retention of cisplatin in the tumor observed for L- and D-CDDP/m may enhance their antitumor efficacy. Therefore, to evaluate the therapeutic ability of the series of CDDP/m, the micelles were intravenously injected three times at 2-day interval to mice bearing subcutaneous BxPC3 tumors and, thereafter, the volume of the tumor was followed for 20 days. L- and D-CDDP/m effectively suppressed the tumor growth, maintaining the initial size of the tumors for more than 20 days, whereas the therapeutic efficacy of D,L-CDDP/m was significantly lower, yet it revealed suppressive effect in tumor growth compared to control (PBS) (Figure 6g). Because the *in vitro* cytotoxicity of the series of CDDP/m was similar regardless of the core conformation (Figure S9 and Table S4, Supporting Information), the observed difference in the antitumor efficacy can be correlated with the enhanced cisplatin exposure by L- and D-CDDP/m to the tumor tissue (Figure 6f). This evident difference in the antitumor efficacy between L- or D-CDDP/m and D,L-CDDP/m may be also elicited by the cumulative delivery of cisplatin in tumor tissues, as the micelles were intravenously injected three times in therapeutic experiments. Consequently, the highly ordered structure in the core of CDDP/m favorably affected their *in vivo* biological performance, as the control of drug release, stability and erosion-like disassembly provided by the α-helices in the core advantageously extended their bioavailability, while avoiding nonspecific biodistribution, and increased accumulation and efficacy against tumors. These observations corresponded with the outstanding performance of CDDP/m as safe and potent nanomedicines in clinical trials ongoing for the treatment of pancreatic tumor,[17,20,39] suggesting the crucial roles of the core-forming α-helix bundles in their appealing performance. Therefore, introducing higher-order assemblies of secondary structures to the basal structure of polymeric micelles may be a potent approach for overcoming *in vivo* hurdles resulting from short half-life in the bloodstream and nonspecific biodistribution due to possible disassembly of the micelles in an uncontrollable manner.

## CONCLUSIONS

Our findings highlight the role of secondary structures of the P(Glu) blocks in the core of CDDP/m on their self-assembly process, physicochemical properties and performance as drug delivery systems. Such higher-order assembly of secondary structures modulated the drug release and disassembly process of the micelles in physiological conditions, improving their plasma half-life and tumor-targeting efficiency. This approach to regulate the micellar functionalities through the formation of higher-ordered hierarchical structures in their core provides a novel concept in polymeric micellar nanomedicines with practical significance particularly in systemic application, where the balance between stability during blood circulation and functionality at targeted sites is always an issue.

## EXPERIMENTAL SECTION

**Materials, Cells, and Animals.** Information regarding materials, cells [human pancreatic cancer (BxPC3) cells] and animals (BALB/c nu/nu, female, 6 weeks old) is described in the Supporting Information. All animal experiments were performed in accordance with the Guidelines for the Care and Use of Laboratory Animals as stated by The University of Tokyo.

**Synthesis of Polymers.** A series of PEG-*b*-P(Glu) block copolymers were synthesized in accordance with the previously described synthetic method with a minor modification.[20] Briefly, *N*-Carboxyanhydride of γ-benzyl L-glutamate (NCA-BLG) was polymerized in 1 M thiourea/DMSO with a macroinitiator PEG-$NH_2$ ($M_w$ = 12000) at room temperature for 5 days. The polydispersity ($M_w/M_n$) of the obtained PEG-*b*-poly(γ-benzyl L-glutamate) (PEG-*b*-PBLG) was estimated by gel permeation chromatography (GPC). The benzyl groups in the PEG-*b*-PBLG were deprotected by mixing with 0.5 N NaOH aqueous solution (5-fold molar excess *vs* benzyl ester units) at room temperature to obtain PEG-*b*-poly(L-glutamic acid) (L-Polymer). Complete deprotection and degree of polymerization of the poly(L-glutamate) blocks was confirmed by proton nuclear magnetic resonance ($^1$H NMR) spectroscopy in $D_2O$ at 25 °C using JNM-ECS400 (JEOL Inc., Tokyo, Japan). PEG-*b*-(D-glutamic acid) (D-Polymer) and PEG-*b*-(D,L-glutamic acid) (D,L-Polymer) were synthesized and characterized in the same manner using *N*-carboxyanhydride of γ-benzyl D-glutamate (NCA-BDG) and the equimolar mixture of NCA-BLG and NCA-BDG, respectively. The detailed

experimental procedure is described in the Supporting Information.

**Self-Assembly Process.** UV and CD spectra were recorded on an UV−vis spectrometer [JASCO V-670DS (Jasco, Tokyo, Japan)] and a CD spectrometer [JASCO710 (Jasco, Tokyo, Japan)], respectively. The scattered light intensity was measured on a Photal dynamic laser scattering spectrometer [DLS-8000 (Otsuka Electronics Co., Ltd., Osaka, Japan); laser: He/Ne (632.8 nm); detection angle: 90°], and the observed scattered light intensity was converted to excess Rayleigh ratio [$\Delta R(90°)$], which is proportional to the weight-averaged molecular weight of the solutes and their concentration.[21] All the experiments were performed at 37 °C. The detailed experimental procedure is described in the Supporting Information.

**Preparation of CDDP/m.** CDDP/m consisting of a series of PEG-*b*-P(Glu) were prepared according to the previously described method with a slight modification.[20] Briefly, a mixture of L-Polymer and CDDP ([Glu] = [CDDP] = 5 mM) in water was stirred for 120 h at 37 °C to prepare L-CDDP/m. The micelles were purified by ultrafiltration [molecular weight cutoff size (MWCO): 30 000], and then passed through 0.22 $\mu$m PVDF filters. D-CDDP/m and D,L-CDDP/m were prepared in the same manner from D-Polymer and D,L-Polymer, respectively.

**Determination of Platinum Concentration.** For micelle solutions, acid digestion was performed with 90% $HNO_3$ followed by dilution with 1% $HNO_3$. The concentration of platinum was determined by inductively coupled plasma mass spectrometry (ICP-MS) [Hewlett-Packard HP 7700 ICP-MS (Agilent Technologies, California, USA). The detailed condition of measurements is described in the Supporting Information.

**Dynamic Light Scattering.** Hydrodynamic diameter and polydispersity index of micelles were estimated based on cumulant expansion of an electric field autocorrelation function measured on the DLS-8000. The detailed experimental procedure is described in the Supporting Information.

**Transmission Electron Microscopy (TEM).** The core structure of micelles was observed through a transmission electron microscopy [JEM1400 (JEOL Inc., Tokyo, Japan); accelerating voltage: 120 kV]. The detailed experimental procedure is described in the Supporting Information.

**Determination of Molecular Weight.** The molecular weight of micelles was estimated by both sedimentation velocity (SV) method and sedimentation equilibrium (SE) method for 0.50 mg/mL micelles in 0.050 M $Na_2SO_4$ aqueous solution using analytical ultracentrifuge [Optima XL-1 (Beckman Coulter, Inc., California, USA)]. For the SV method, acquired sedimentation boundaries were fitted based on Lamm equation using continuous molecular weight distribution model on SEDFIT software for calculating the distribution of molecular weight,[26] from which both weight- and number-averaged molecular weight of the samples were calculated. Partial specific volume of the micelles, which is required for the determination of molecular weight, was calculated based on the density of series dilution of the micelle solution measured on a densimeter [DMA 4500 (Anton Paar GmbH, Graz, Austria)]. The detailed experimental procedure is described in the Supporting Information.

**Determination of α-Helical Content.** The mean residue ellipticity at 222 nm ($[\theta]_{222}$) on the CD spectrum of micelles was utilized to estimate the α-helical content (% helix) of the P(Glu) blocks constituting the core of the micelles according to the following equation:[40,41]

$$\%\text{helix} = \frac{[\theta]_{222} - [\theta]_{222,\,R}}{[\theta]_{222,\,H} - [\theta]_{222,\,R}} \times 100$$

where $[\theta]_{222,R}$ and $[\theta]_{222,H}$ are the mean residue ellipticity at 222 nm of poly(L-glutamic acid) consisting of 40 glutamate units in 100% random coil and 100% α-helix conformation,[41,42] respectively. For D-CDDP/m, the sign of the obtained signal was reversed to use this equation.

**Small Angle X-ray Scattering (SAXS).** SAXS measurements of micelles were performed by using a FR-X/BioSAXS-1000 [Rigaku, Tokyo, Japan; incident beam: Cu Kα ($\lambda$ = 1.54187 Å)] at a concentration range from 10 to 50 mg/mL. The scattering vector ($q$) *vs* intensity ($I(q)$) curves (SAXS profiles) of pure water was subtracted from the SAXS profiles of micelles. The detailed experimental procedure is described in the Supporting Information.

**Disintegration of Micelles in Physiological Condition.** Release of cisplatin and disassembly of micelles were followed in phosphate buffered saline [10 mM phosphate buffer containing 150 mM NaCl (pH 7.4)] in the dark at 37 °C by various methods as follows. The release of cisplatin from micelles was examined by dialyzing the micelles toward PBS, and the amount of released platinum at defined time points was quantified by ICP-MS. The disassembly of micellar structure and the variation in secondary structure in the P(Glu) blocks were followed by scattered light intensity and CD spectra, respectively. For the detailed study on the disassembly process, the micelles were incubated in PBS for defined time periods and dialyzed toward 50 mM $Na_2SO_4$ aqueous solution to remove free drug and PBS. Thereafter, the solution was analyzed by SV method of analytical ultracentrifugation. The detailed experimental procedure is described in the Supporting Information.

**Plasma Clearance and Biodistribution.** BALB/c nu/nu mice bearing BxPC3 tumors ($n$ = 6) were intravenously administered with a series of CDDP/m at a dose of 100 $\mu$g/mouse on a CDDP basis. Mice were sacrificed 1, 4, 8, 24, and 48 h after the administration. The blood was collected from the inferior vena cava using heparinized syringes and centrifuged to obtain the plasma and blood cells. At the same time, the tumor, liver, spleen, kidney were excised and washed with phosphate buffered saline. All samples were weighed, and then acid digestion was performed with 90% $HNO_3$. The platinum concentration was measured by ICP-MS after redissolving the samples in 1% $HNO_3$ at the proper dilution rate. Statistical significance among the groups was estimated by two-way analysis of variance (ANOVA). The two-tailed $P$ value less than 0.05 was considered to indicate statistical significance.

**Antitumor Efficacy.** BALB/c nu/nu mice bearing BxPC3 tumors ($n$ = 6) were given in total three intravenous administrations of a series of CDDP/m at a dose of 4 mg/kg on a CDDP basis, with each administration at two-day intervals. To quantify the antitumor efficacy, the tumor volume ($V$) was measured according to the following equation:

$$V = \frac{a \times b^2}{2}$$

where $a$ and $b$ are the major and minor axes of the tumor, respectively, measured with a caliper. The tumor volume at each day was normalized against the initial day. Statistical significance among the groups was estimated by two-way analysis of variance (ANOVA). The two-tailed $P$ value less than 0.05 was considered to indicate statistical significance.

***In Vitro* Cytotoxicity.** The experimental procedure is described in the Supporting Information.

*Conflict of Interest:* The authors declare no competing financial interest.

*Acknowledgment.* This study was supported by the Funding Program for World-Leading Innovative R&D on Science and Technology (FIRST Program) from the Japan Society for the Promotion of Science (JSPS) (K.K.), Center of Innovation Science and Technology based Radical Innovation and Entrepreneurship Program (COI STREAM) from the Ministry of Education, Culture, Sports, Science and Technology (MEXT) (K.K.), Research on Publicly Essential Drugs and Medical Devices from Japan Health Sciences Foundation (N.N.), Takeda Science Foundation (N.N.), Precursory Research for Embryonic Science and Technology (PRESTO) from the Japan Science and Technology Corporation (JST) (K.O.), as well as Grants-in-Aid for JSPS for Young Scientists (H.C., Y.M.). Additional support was provided by Grants-in-Aid for JSPS Fellows (Y.M). Transmission electron microscopy studies were conducted at Research Hub for Advanced Nano Characterization, The University of Tokyo, supported by MEXT. The measurements of small-angle X-ray scattering were kindly performed by Rigaku Corporation at X-ray Research Laboratory, Rigaku Corporation (Tokyo, Japan).

*Supporting Information Available:* Experimental details, supporting figures regarding characterization of the synthesized

polymers, variation in UV spectra during micelle formation, CD spectra of L-Polymer at pH 5.2, molecular model of cisplatin-conjugated poly(L-glutamic acid), second derivative SAXS spectra of L-CDDP/m, form factor of core−shell particles applied to L-CDDP/m and cytotoxicity of CDDP/m, a supporting scheme illustrating diffraction planes and interhelical distance in hexagonally aligned α-helices and structural dimension of the proposed model of L-CDDP/m and supporting tables summarizing the scattering vector at the peak of SAXS profiles, experimental and calculated molecular weight of unimers and dimers resulted from disintegration of CDDP/m, and PEG density and *in vitro* cytotoxicity of CDDP/m. This material is available free of charge *via* the Internet at http://pubs.acs.org.

## REFERENCES AND NOTES


1. Allen, C.; Maysinger, D.; Eisenberg, A. Nano-Engineering Block Copolymer Aggregates for Drug Delivery. *Colloids Surf., B* **1999**, *16*, 3–27.
2. Haag, R. Supramolecular Drug-Delivery Systems Based on Polymeric Core-Shell Architectures. *Angew. Chem., Int. Ed. Engl.* **2004**, *43*, 278–282.
3. Rodriguez-Hernandez, J.; Checot, F.; Gnanou, Y.; Lecommandoux, S. Toward "Smart" Nano-Objects by Self-Assembly of Block Copolymers in Solution. *Prog. Polym. Sci.* **2005**, *30*, 691–724.
4. Harada, A.; Kataoka, K. Supramolecular Assemblies of Block Copolymers in Aqueous Media as Nanocontainers Relevant to Biological Applications. *Prog. Polym. Sci.* **2006**, *31*, 949–982.
5. Carlsen, A.; Lecommandoux, S. Self-Assembly of Polypeptide-Based Block Copolymer Amphiphiles. *Curr. Opin. Colloid Interface Sci.* **2009**, *14*, 329–339.
6. Zayed, J. M.; Nouvel, N.; Rauwald, U.; Scherman, O. A. Chemical Complexity—Supramolecular Self-Assembly of Synthetic and Biological Building Blocks in Water. *Chem. Soc. Rev.* **2010**, *39*, 2806–2816.
7. Shu, J. Y.; Panganiban, B.; Xu, T. Peptide-Polymer Conjugates: From Fundamental Science to Application. *Annu. Rev. Phys. Chem.* **2013**, *64*, 631–657.
8. Vandermeulen, G. W. M.; Klok, H.-A. Peptide/Protein Hybrid Materials: Enhanced Control of Structure and Improved Performance through Conjugation of Biological and Synthetic Polymers. *Macromol. Biosci.* **2004**, *4*, 383–398.
9. Carlsen, A.; Lecommandoux, S. Self-Assembly of Polypeptide-Based Block Copolymer Amphiphiles. *Curr. Opin. Colloid Interface Sci.* **2009**, *14*, 329–339.
10. Osada, K.; Kataoka, K. Drug and Gene Delivery Based on Supramolecular Assembly of PEG-Polypeptide Hybrid Block Copolymers. *Adv. Polym. Sci.* **2006**, *202*, 113–153.
11. Kataoka, K.; Harada, A.; Nagasaki, Y. Block Copolymer Micelles for Drug Delivery: Design, Characterization and Biological Significance. *Adv. Drug Delivery Rev.* **2001**, *47*, 113–131.
12. Kataoka, K.; Kwon, G. S.; Yokoyama, M.; Okano, T.; Sakurai, Y. Block Copolymer Micelles as Vehicles for Drug Delivery. *J. Controlled Release* **1993**, *24*, 119–132.
13. Nishiyama, N.; Kataoka, K. Current State, Achievements, and Future Prospects of Polymeric Micelles as Nanocarriers for Drug and Gene Delivery. *Pharmacol. Ther.* **2006**, *112*, 630–648.
14. Osada, K.; Christie, R. J.; Kataoka, K. Polymeric Micelles from Poly(ethylene glycol)-Poly(amino acid) Block Copolymer for Drug and Gene Delivery. *J. R. Soc. Interface* **2009**, *6*, S325–S339.
15. Matsumura, Y. Preclinical and Clinical Studies of NK012, an SN-38-Incorporating Polymeric Micelles, Which Is Designed Based on EPR Effect. *Adv. Drug Delivery Rev.* **2011**, *63*, 184–192.
16. Matsumura, Y.; Kataoka, K. Preclinical and Clinical Studies of Anticancer Agent-Incorporating Polymer Micelles. *Cancer Sci.* **2009**, *100*, 572–579.
17. Plummer, R.; Wilson, R. H.; Calvert, H.; Boddy, A. V.; Griffin, M.; Sludden, J.; Tilby, M. J.; Eatock, M.; Pearson, D. G.; Ottley, C. J.; *et al.* A Phase I Clinical Study of Cisplatin-Incorporated Polymeric Micelles (NC-6004) in Patients with Solid Tumours. *Br. J. Cancer* **2011**, *104*, 593–598.
18. Imahori, K.; Tanaka, J. Ultraviolet Absorption Spectra of Poly-L-Glutamic Acid. *J. Mol. Biol.* **1959**, *1*, 359–364.
19. Lader, H. J.; Komoroski, R. A.; Mandelkern, L. A Nuclear Magnetic Resonance Study of the Helix-Coil Transition of Poly(L-glutamic acid). *Biopolymers* **1977**, *16*, 895–905.
20. Nishiyama, N.; Okazaki, S.; Cabral, H.; Miyamoto, M.; Kato, Y.; Sugiyama, Y.; Nishio, K.; Matsumura, Y.; Kataoka, K. Novel Cisplatin-Incorporated Polymeric Micelles Can Eradicate Solid Tumors in Mice. *Cancer Res.* **2003**, *63*, 8977–8983.
21. Schärtl, W. *Light Scattering from Polymer Solutions and Nanoparticle Dispersions*; Springer-Verlag: Berlin, 2007.
22. Vincenzo, B.; Vittorio, C.; Luca, M.; Franco, S. Photochemistry of Coordination Compounds. XIII. Photochemical Behavior and Electronic Spectra of Some $d^8$ Glycinato Complexes. *Inorg. Chem.* **1965**, *4*, 1243–1247.
23. Nishiyama, N.; Yokoyama, M.; Aoyagi, T.; Okano, T.; Sakurai, Y.; Kataoka, K. Preparation and Characterization of Self-Assembled Polymer-Metal Complex Micelle from *cis*-Dichlorodiammineplatinum(II) and Poly(ethylene glycol)-Poly(α,β-aspartic acid) Block Copolymer in an Aqueous Medium. *Langmuir* **1999**, *15*, 377–383.
24. Kuntz, I. D. Hydration of Macromolecules. III. Hydration of Polypeptides. *J. Am. Chem. Soc.* **1971**, *93*, 514–516.
25. Yotsuyanagi, T.; Usami, M.; Noda, Y.; Nagata, M. Computational Consideration of Cisplatin Hydrolysis and Acid Dissociation in Aqueous Media: Effect of Total Drug Concentrations. *Int. J. Pharm.* **2002**, *246*, 95–104.
26. Schuck, P. Size-Distribution Analysis of Macromolecules by Sedimentation Velocity Ultracentrifugation and Lamm Equation Modeling. *Biophys. J.* **2000**, *78*, 1606–1619.
27. Pauling, L.; Corey, R. B.; Branson, H. R. The Structure of Proteins: Two Hydrogen-Bonded Helical Configurations of the Polypeptide Chain. *Proc. Natl. Acad. Sci. U. S. A.* **1951**, *37*, 205–211.
28. Bellomo, E. G.; Wyrsta, M. D.; Pakstis, L.; Pochan, D. J.; Deming, T. J. Stimuli-Responsive Polypeptide Vesicles by Conformation-Specific Assembly. *Nat. Mater.* **2004**, *3*, 244–248.
29. Rodríguez-Hernández, J.; Lecommandoux, S. Reversible Inside-Out Micellization of pH-Responsive and Water-Soluble Vesicles Based on Polypeptide Diblock Copolymers. *J. Am. Chem. Soc.* **2005**, *127*, 2026–2027.
30. Osada, K.; Cabral, H.; Mochida, Y.; Lee, S.; Nagata, K.; Matsuura, T.; Yamamoto, M.; Anraku, Y.; Kishimura, A.; Nishiyama, N.; *et al.* Bioactive Polymeric Metallosomes Self-Assembled through Block Copolymer-Metal Complexation. *J. Am. Chem. Soc.* **2012**, *134*, 13172–13175.
31. Lund, R.; Shu, J.; Xu, T. A Small-Angle X-Ray Scattering Study of α-Helical Bundle-Forming Peptide-Polymer Conjugates in Solution: Chain Conformations. *Macromolecules* **2013**, *46*, 1625–1632.
32. Floudas, G.; Papadopoulos, P. Hierarchical Self-Assembly of Poly (γ-benzyl-L-glutamate)-Poly (ethylene glycol)-Poly (γ-benzyl-L-glutamate) Rod-Coil-Rod Triblock Copolymers. *Macromolecules* **2003**, *36*, 3673–3683.
33. Lau, S. Y. M.; Taneja, A. K.; Hodges, S. Synthesis of a Model Protein of Defined Secondary and Quaternary Structure. *J. Biol. Chem.* **1984**, *259*, 13253–13261.
34. Matsumura, Y.; Maeda, H. A New Concept for Macromolecular Therapeutics in Cancer Chemotherapy: Mechanism of Tumoritropic Accumulation of Proteins and the Antitumor Agent Smancs. *Cancer Res.* **1986**, *46*, 6387–6392.
35. Choi, H. S.; Liu, W.; Misra, P.; Tanaka, E.; Zimmer, J. P.; Itty Ipe, B.; Bawendi, M. G.; Frangioni, J. V. Renal Clearance of Quantum Dots. *Nat. Biotechnol.* **2007**, *25*, 1165–1170.
36. Moghimi, S. M.; Hunter, A. C.; Murray, J. C. Long-Circulating and Target-Specific Nanoparticles: Theory to Practice. *Pharmacol. Rev.* **2001**, *53*, 283–318.
37. American Cancer Society. *Cancer Facts & Figures 2011*; American Cancer Society: Atlanta, GA, 2011.

38. Gref, R.; Lück, M.; Quellec, P.; Marchand, M.; Dellacherie, E.; Harnisch, S.; Blunk, T.; Müller, R. 'Stealth' Corona-Core Nanoparticles Surface Modified by Polyethylene Glycol (PEG): Influences of the Corona (PEG Chain Length and Surface Density) and of the Core Composition on Phagocytic Uptake and Plasma Protein Adsorption. *Colloids Surf., B* **2000**, *18*, 301–313.
39. Uchino, H.; Matsumura, Y.; Negishi, T.; Koizumi, F.; Hayashi, T.; Honda, T.; Nishiyama, N.; Kataoka, K.; Naito, S.; Kakizoe, T. Cisplatin-Incorporating Polymeric Micelles (NC-6004) Can Reduce Nephrotoxicity and Neurotoxicity of Cisplatin in Rats. *Br. J. Cancer* **2005**, *93*, 678–687.
40. Greenfield, N.; Fasman, G. D. Computed Circular Dichroism Spectra for the Evaluation of Protein Conformation. *Biochemistry* **1969**, *8*, 4108–4116.
41. Chen, Y. H.; Yang, J. T.; Chau, K. H. Determination of the Helix and $\beta$ Form of Proteins in Aqueous Solution by Circular Dichroism. *Biochemistry* **1974**, *13*, 3350–3559.
42. Cassim, J. Y.; Yang, J. T. Critical Comparison of the Experimental Optical Activity of Helical Polypeptides and the Predictions of the Molecular Exciton Model. *Biopolymers* **1970**, *9*, 1475–1502.